Femtosecond filamentation in sapphire with diffractive lenses

R. Borrego-Varillas,[1,*] C. Romero,[2] O. Mendoza-Yero,[3] G. Mínguez-Vega,[3] I. Gallardo,[2] and J. R. Vázquez de Aldana[4]

[1]*Grupo de Investigación en Óptica Extrema (GIOE), Universidad de Salamanca, E-37008 Salamanca, Spain*
[2]*Centro de Láseres Pulsados CLPU, C/Adaja SN, Edificio M3 Parque Científico, E-37185 Villamayor (Salamanca), Spain*
[3]*GROC·UJI, Insititut de Noves Tecnologies de la Imatge, Universitat Jaume I, E-12080 Castelló, Spain*
[4]*Grupo de Investigación en Microprocesado de Materiales con Láser, Facultad de Ciencias, Universidad de Salamanca, E-37008 Salamanca, Spain*
**Corresponding author: rociobv@usal.es*

Received April 17, 2013; accepted June 7, 2013;
posted June 14, 2013 (Doc. ID 189029); published July 5, 2013

In this paper, we demonstrate novel properties in the phenomenology of supercontinuum generation in sapphire with diffractive lenses and provide a complete spatial, spectral, and temporal characterization of the so-generated pulses. Filament formation inside the sample is analyzed and related to the measured spectra, finding that clipping of the filament results in blueshifted spectra. For comparison, filament formation with refractive lenses is also examined, and the roles of diffraction and extension of the focusing region are inspected. The tunability achieved in the anti-Stokes side of the spectrum is also extended to the ultraviolet by frequency mixing with infrared femtosecond pulses.

OCIS codes: (050.0050) Diffraction and gratings; (320.6629) Supercontinuum generation; (320.7110) Ultrafast nonlinear optics.
http://dx.doi.org/10.1364/JOSAB.30.002059

1. INTRODUCTION

High-power femtosecond laser systems based on Ti:sapphire offer tunability limited to a narrow range around 800 nm. For applications in which other wavelengths are required, parametric nonlinear processes [1] are typically used. Processes such as second-harmonic generation [2] in combination with sum-frequency generation (SFG) in nonlinear crystals allow one to obtain femtosecond pulses at discrete wavelengths at the second, the third, or even the fourth harmonic [3] of the fundamental. Continuous tunability in the visible or in the infrared (IR) can be achieved by optical parametric amplification (OPA) [4], and in the ultraviolet (UV) with a subsequent stage of SFG or with new OPA schemes [5,6].

One of the most widely used methods to obtain the signal pulse necessary to seed ultrafast optical parametric amplifiers is the generation of supercontinuum (SC) in bulk (crystal or glass) [7]. When a high-power IR femtosecond pulse is focused into a transparent solid, different nonlinear effects such as self-focusing, self-phase modulation, self-steepening, plasma generation, or filamentation take place [8]. These effects usually give rise to an extreme spectral broadening of the pulse, ranging from the UV to the IR regions of the spectrum that is termed SC generation [9,10]. The spectral properties of the SC pulses have been shown to depend on several factors. In particular, the extension of blue (anti-Stokes) broadening is strongly related to certain properties of the medium, such as the band-gap [11–13] or its chromatic dispersion [14]. It is also known that some experimental conditions play a crucial role in determining the maximum extension of the spectra, e.g., the numerical aperture (NA) of the incident beam [15,16] or the focus position [17–19].

In a recent paper [20], the possibility to tailor the spectral features of SC pulses generated in bulk (sapphire and fused silica) by using a diffractive lens (DL) as focusing optics was demonstrated [21]. In general, the spectrum of SC pulses generated with DLs exhibited a strongly peaked structure toward the blue extreme of the SC that was particularly stable, and reached very short wavelengths (under 450 nm) in the case of using a sapphire target. The change of the relative distance between the DL and the sapphire crystal was shown to achieve wavelength tunability in the position of the spectral peak. This property was not observed when an achromatic refractive lens (RL) with the same focal length was used for beam focalization under the same irradiation conditions. Moreover, the spectral extension (blue border) of the SC generated with the DL was in all cases larger than the one generated with the achromatic doublet.

In this paper, we demonstrate novel properties in the phenomenology of white light generation in sapphire with DLs, and provide a deep study of the so-generated pulses. For this purpose, we experimentally study the dynamics of the filament created inside the bulk. The spectral properties of the SC are related to the development of the filament. For comparison, filament formation with refractive lenses is also examined and the roles of diffraction and extension of the focusing region are inspected. In a second part, we present a detailed study of the spatial, spectral, and temporal features of these SC pulses to assess their usefulness for further applications. In particular, the intensity profile, beam quality,

focusability, temporal duration, and spatial chirp are reported. Finally, we demonstrate that the tunability accomplished in the blue part of the spectrum can also be extended to the UV by the frequency mixing process. The spectral control that can be achieved using the DL and the reported properties makes this kind of pulse very interesting for seeding UV–VIS OPAs or for other direct applications such as interferometry, optical coherence tomography, frequency metrology, or fluorescence lifetime imaging.

2. EXPERIMENTAL SETUP

The experimental setup used to produce the SC pulses was the same in all the cases studied throughout this work, and it is depicted in Fig. 1. A Ti:sapphire regenerative amplifier (Spitfire, Spectra Physics) was the laser source. It delivered pulses of 120 fs full width at half-maximum (FWHM) at a central wavelength of 795 nm (spectral width 10 nm) and operated at a repetition rate of 1 kHz. The mean beam power was measured with an analog power meter (Spectra Physics, Model 407-A) and was adjusted with a half-wave plate and a linear polarizer. An additional calibrated neutral-density filter allowed us to reduce the absolute error in the power measurements. Previously to the realization of the experiments, the laser compressor was adjusted in order to compensate for dispersion in all the optical elements placed before the lens. This adjustment was performed using a GRENOUILLE (Swamp Optics) for temporal retrieval of the pump pulses.

The optical element used to focus the beam into the sample was a kinoform DL (Institute of Automatics and Electrometry, Russia) with a focal length of $f_o = 106.6$ mm for $\lambda_o = 795$ nm. This DL has an efficiency of 69% for the central wavelength λ_o. Due to their diffractive nature, DLs exhibit a strong chromatic aberration resulting in the following dependence of the focal length on the wavelength λ of the incident light:

$$f(\lambda) = \frac{f_0 \lambda_0}{\lambda}, \tag{1}$$

where f_o is the focal length for the wavelength λ_o. As discussed in [20,22], for the wide spectral bandwidth of femtosecond pulses, we can define an extended focal region Δf as the distance along the propagation axis between the foci of the extreme wavelengths of a laser with spectral bandwidth $\Delta\lambda$. It can be determined from Eq. (1) as $\Delta f = f_o \Delta\lambda/\lambda_o$. In our experimental conditions the extended focal region is $\Delta f \sim 1.3$ mm.

An iris aligned with the beam was placed in front of the lens. This iris was used in some experiments to reduce the NA by limiting the beam size, thus increasing the Rayleigh range. For our studies, we have used as a target a circular sapphire plate (Eksma Optics) of 3 mm thickness oriented with the optical axis parallel to the laser polarization. It was placed over a motorized linear stage to obtain an accurate control of its position along the propagation direction (z).

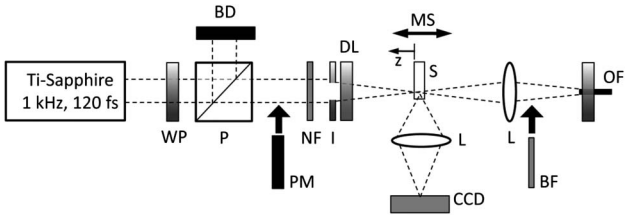

Fig. 1. Experimental setup for SC generation. WP, half-wave plate; P, linear polarizer; PM, power meter; BD, beam dumper; NF, neutral-density filter; I, iris; DL, kinoform diffractive lens; MS, motorized linear stage; S, sample (sapphire); L, lens; OF, optical fiber.

In order to analyze the filament generated inside the crystal during SC generation, the circular border of the sample was partially polished up to optical quality. An $f = 100$ mm lens (Thorlabs, AC254-100-B) was used to image the filament onto a digital CMOS camera (IDS, uEye UI-1480SE-C USB2). According to the point-spread function of the lens, the resolving power for this imaging system was estimated to be 3.5 μm, which is enough to resolve the filament's profile. Calibration of the image dimensions (pixels/mm) was performed by moving the sample a known quantity along the z axis with the translational stage. The displacement was then measured in terms of pixels with the software provided with the CCD, and the equivalence in length units (mm) was performed. Measurements of the spectra of SC pulses were perormed by focusing the generated pulse with a convergent lens (AC245-045-A1 Thorlabs, $f = 45$ mm) some millimeters before the input coupling of a 50 μm core optical fiber (Ocean Optics, P50-2-UV-VIS). In this way, most of the light exiting the crystal is collected, whereas the large NA of the fiber ensures that the pulse is correctly coupled into the fiber. The nonconverted IR light was removed by means of a band-pass filter (Thorlabs, FG37S), whose transmittance was characterized experimentally. The spectrometer used for this purpose was an AvaSpec-2048 (Avantes). A previous calibration of the spectrometer's sensitivity was made by means of a calibration lamp (Ocean Optics, LS-1-CAL).

To measure absolute spectral densities, we used a power meter (Newport, 1830-C). Although its sensitivity matches our range of interest, this model is wavelength dependent and therefore it is not possible to directly integrate all the spectral components of the SC. To overcome this limitation we used interference filters, which were previously calibrated with a calibration lamp (LS-1-CAL, Ocean Optics). This allowed us to experimentally measure their transmittance $T(\lambda)$, as well as their spectral bandwidth.

The power meter measures the energy (U) passing through an interference filter, which can be expressed as

$$U = U_0 \int T(\lambda)\bar{S}(\lambda)\mathrm{d}\lambda, \tag{2}$$

$T(\lambda)$ being the transmission function of the interference filter, $S(\bar{\lambda})$ the normalized spectrum (arbitrary units), and U_0 the peak spectral density (nJ/nm). To convert the spectrum in arbitrary units (as measured by the spectrometer) to spectral densities (nJ/nm), $S(\lambda) = U_0\bar{S}(\lambda)$, we solve Eq. (2) numerically.

In order to obtain a more accurate measurement, we used six interference filters for the visible range (models 6471 3C JAV2-1, 5777 3C ETS 2-0, 546 0759, 35-3474 T-BEZ, and 35-3334 5192 from EALING, and P10-515-S 93819 from CORION) and averaged the values obtained for U_0 with each of them.

3. EXPERIMENTAL RESULTS

Prior to the measurements, we determined the threshold for SC generation under the experimental conditions used in this work. This is done by focusing the pulse in the sapphire plate

and visually inspecting the beam projected on a white paper screen at the output of the sample. We take as threshold the minimum power (or pulse energy) at which some visible light is generated for any position of the crystal (a scan is done around the focus with the motorized stage). In all cases when SC was generated, a filament was formed inside the bulk whose plasma emission could be seen with the naked eye. For the DL, the threshold energy of the incident laser pulses for SC generation was $E_{\text{th}} = 0.95$ μJ (value estimated after the DL, considering the efficiency of the lens and the transmittance of the neutral-density filter). In order to avoid multiple filamentation and to minimize the damage of the sapphire crystal, in all measurements performed in this work (unless otherwise specified), the energy of the incident pulses was taken slightly over this value ($\sim 1.4E_{\text{th}}$).

A. Filament Formation

We have first analyzed plasma emission of the filament generated in the sapphire sample, with the image-forming system and the CCD, in terms of the position of the sapphire plate along the z (propagation) axis. At the same time, the spectrum of the generated SC was recorded with the spectrometer. Results are presented in Fig. 2, where we have defined $z = 0$ as the position of the crystal at which some SC generation was first observed. Increased values of z correspond to shorter relative distances of the DL sample. When the IR femtosecond pulse is focused in the sample slightly behind the first interface, a filament extending around 1.5 mm develops (see Fig. 2, picture at the top). This length is just 0.2 mm larger than the previously defined extended focal region. A careful inspection of the intensity profile along the filament suggests the existence of a refocusing process: the profile does not exhibit a monotonically decreasing

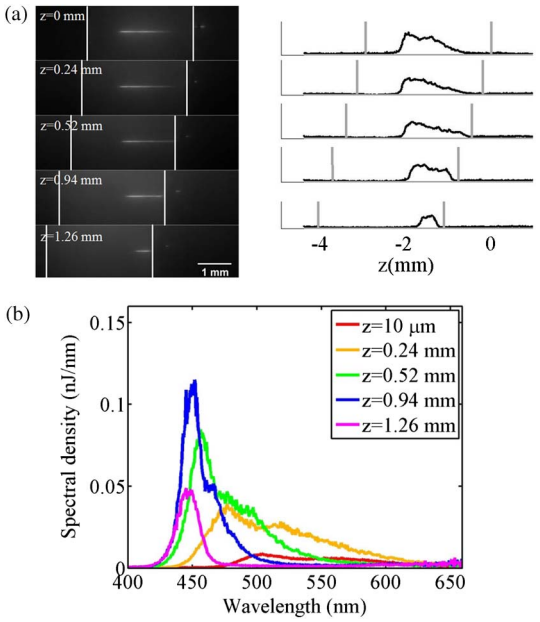

Fig. 2. (a) Pictures of the filament produced by the DL inside the sapphire sample (input and output faces marked with vertical lines) at different positions of the crystal along the propagation. The pulse propagates from left to right, and the energy was set to 1.30 μJ. Profiles shown near each picture correspond to an intensity cut along the filament axis. (b) Spectra of the generated SC pulses for different positions of the sapphire crystal.

intensity after the main peak, and, on the contrary, it slightly increases again previously to a smooth decrease. The spectrum of the SC generated in these conditions shows a peaked structure with a maximum around 500 nm that abruptly drops toward shorter wavelengths. The structure of both the SC spectral intensity and the plasma emission profile remains quite stable if we change by a few hundred micrometers the position of the sample along the z axis, though the spectral density increases as we approach the DL.

A significant change appears when the sample is moved even more toward the lens [Fig. 2(b)]. Then, the extension of the filament is clipped due to the presence of the end face of the sapphire. The spectrum of the SC shows a narrower and bluer peak than in previous cases. As we continue approaching the crystal to the DL, this effect is more pronounced, leading finally to a narrow blue peak (20 nm FWHM) centered at a wavelength of 446 nm when the filament formation is strongly clipped.

Similar studies have been performed previously [19] using a concave mirror to focus the femtosecond pulse in a fused-silica sample. The sample was moved around the focal point and the spectra of the output pulses were analyzed. It was clearly demonstrated, with both experimental measurements and numerical simulations, that the extension of the spectrum toward shorter wavelengths increases with the filament extension. When the filament length was not clipped by the output face of the sample, the spectra showed the largest extension. Similar results were also reported for water by Ziolek *et al.* [17].

The results we obtained with the DL seem to be contradictory to those observations: we obtained the shorter wavelengths when the filament extension was strongly clipped by the output face of the sapphire plate, although the total spectral content in this case was smaller because the spectrum exhibits just a narrow peak structure in the blue.

In order to elucidate whether the observed new results are due to the longer extension of the Rayleigh length or not, we have performed a set of experiments by replacing the DL with an achromatic RL (Linos G063144525) with $f = 100$ mm. For comparison with the DL, the extension of the focusing region must be analogous. Therefore, a proper iris size for the RL must be estimated. For this reason, we first experimentally determined the focusing region of the DL in the linear regime in air. For this purpose, we monitored the beam profile around the focus with a high-resolution CMOS-based camera (uEye, UI-1460-C) mounted on a motorized stage (Zaber, T-LA28). We adopted the criterion of the distance between points at which intensity drops to half of the maximum as an extension of the focusing region [23]. We found a focusing length of $\Delta z \sim 1.9$ mm for the DL. Following a similar procedure, a similar focusing region was found for the RL when the iris placed in front of the lens was reduced to 5.5 mm (diameter).

In order to keep similar conditions ($\sim 1.4E_{\text{th}}$) to those with the DL, the pulse energy was set to 0.98 μJ. In such conditions, a set of measurements was performed while scanning the sapphire crystal in the vicinity of the focus. Results are shown in Fig. 3. As can be seen in the images, the length of the filament was shorter in all cases than that produced with the DL. The depth of the sample at which the filament develops for the different positions of the crystal also exhibits a different trend

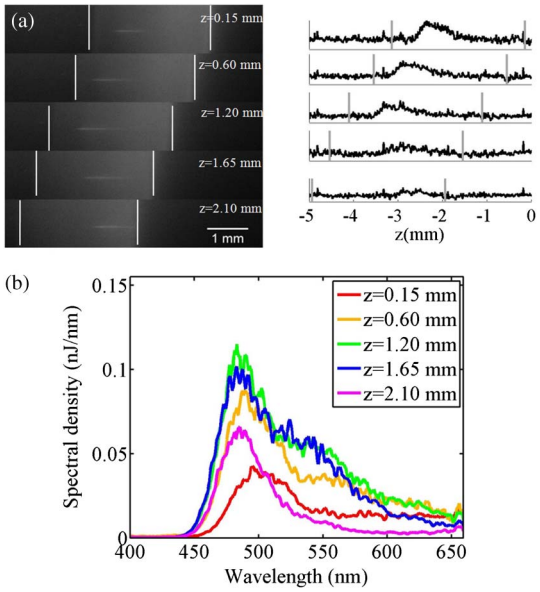

Fig. 3. (a) Pictures of the filament produced inside the sapphire sample (input and output faces marked with vertical lines) at different positions of the crystal along the propagation axis when a RL ($f = 100$ mm) was used to focus the pulsed beam. An iris with a diameter of 5.5 mm was placed in front of the lens. The pulse propagates from left to right, and the energy was set to 0.98 μJ. Profiles shown near each picture correspond to an intensity cut along the filament axis. (b) Spectra of the generated SC pulses for different positions of the sapphire crystal.

than that shown for the DL: the beginning of the filament now moves forward as the crystal is moved in the same direction. At a certain distance the behavior saturates and then the clipping of the rear part of the filament begins, due to the output face of the crystal. Concerning the spectrum of the SC pulses, we see that the clipping of the filament affects only the spectral content in the longer wavelength part: as the filament is more strongly clipped, the spectrum becomes narrower, but the minimum wavelength and the position of the main peak remain unchanged. Moreover, the minimum wavelength obtained in the SC is larger than that obtained when the DL was used.

Thus, we suggest that the complex spectral and temporal dynamics of an ultrashort laser pulse focused by a DL are crucial for the behavior reported in Fig. 2 to occur, and not only the extension of the focal length. In [24] a complete study of the pulses focused by this DL (i.e., our pump pulses for SC generation) is presented in the linear regime in air. That work shows the particular dependence of both the wavelength and the pulse duration on the axis position near the focus, and the different temporal chirps in front of or behind the focus f_0 for the central wavelength.

Material dispersion and initial pulse chirp have been demonstrated to play a crucial role in SC spectral shaping. In particular, Kartazaev and Alfano reported a strong and sharp spectral peak in the anti-Stokes side of SC generated in calcite by stretching 80 fs pulses ($\lambda = 800$ nm) to 130 fs [25]. The wavelength of this spectral peak was tuned by introducing chirp (negative and positive) and changing pulse energy. On the other hand, Faccio *et al.* achieved a tunable, extremely blueshifted continuum in silica with $\lambda = 1.055$ μm pulses (normal group-velocity dispersion regime) [26], which was explained in terms of X waves: the blue spectral peak was shown to be the blueshifted tail of the same pump X wave formed in the filament. The tunability of the blue peak was achieved by moving the silica sample toward the lens; similar to our results with the DL, the anti-Stokes wing in such a case moved toward shorter wavelengths as the sample was approaching the lens. More recently, Smetanina *et al.* have demonstrated the formation of a peaked structure in the anti-Stokes side in SC generation in fused silica as a consequence of the peculiarity of filamentation in the anomalous dispersion regime [27]. The formation of this anti-Stokes wing is interpreted as a result of strong pulse self-steepening and destructive interference of the broadband SC in the band located between the isolated anti-Stokes wing and the broadened pulse spectrum.

We think that in such particular dynamics of the pulse focused by a DL, the dispersion introduced by the material prior to the filament formation could, to some extent, lead to an intensity increase that pushes the spectral components of the SC more deeply toward the blue as the crystal is moved toward the lens.

B. Spatial and Spectral Characterization

In the spectral measurements shown in the previous subsection, the SC pulse was concentrated with a convergent lens so that all the angular components of the generated pulse were collected and included in the spectral profiles. We now present measurements of the angular dependence of the generated spectrum (i.e., the spatial chirp). To this end, we placed the input coupling of the optical fiber in a motorized linear stage moving in the plane perpendicular to the propagation axis, 200 mm behind the geometrical focus of the DL. The SC pulse emerging from the crystal was directly coupled in the spectrometer so that the position of the fiber coupling allowed us to calculate the emergence angle. The sapphire sample was placed at $z = 1.3$ mm in order to get the shortest wavelengths, and the energy was set to 1.30 μJ. Results are shown in Fig. 4.

As can be seen in Fig. 4(a), the spectrum of the SC pulse is nearly the same for all the emergence angles. The only significant difference is a slight increase in the width of the spectral peak toward the center of the beam. From this measurement we can extract the NA of the beam, which is ~0.02.

In Fig. 4(b) we show the spectral map of the SC generated when the iris placed in front of the lens is closed to a diameter of 5.5 mm, thus reducing the NA of the incident IR pulse to ~0.026. The pulse energy was set to 0.9 μJ in order to perform the experiment at the same $1.4E_{\text{th}}$ condition, and the sample was placed 1.9 mm behind the DL. In this case, the central wavelength of the spectral peak increases. The angular dependence of the spectrum is negligible, and the NA is again ~0.02.

The spatial quality of the beam was analyzed in a subsequent set of experiments. A lens of $f = 4.5$ mm (Thorlabs, AC254-045-A1) was used to collimate the SC beam generated when the sapphire crystal was placed at $z = 1.2$ mm, and the pulse energy of the IR was $E = 1.3$ μJ. The nonconverted part of the IR pulses was removed by using a band-pass filter (Thorlabs, FG37S). In some cases, an additional neutral-density filter was employed to prevent camera saturation. A second lens of $f = 200$ mm (Thorlabs, AC254-200-A1) was placed to focus the beam, achieving with this configuration a large Rayleigh length and a beam magnification that allowed us to monitor the spatial quality of the beam around the focus.

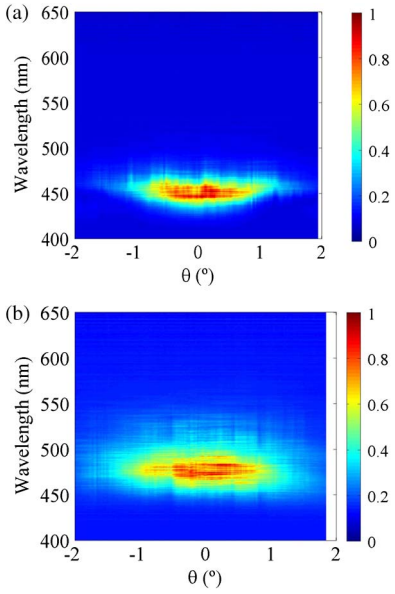

Fig. 4. Angular dependence of the spectrum of SC pulses generated with the DL. The horizontal scale is the angle with respect to the propagation axis. (a) $z = 1.3$ mm and $E = 1.3$ μJ. (b) An iris of 5.5 mm was placed before the lens. $z = 1.9$ mm, $E = 0.9$ μJ.

For this purpose, a CMOS digital camera (IDS, uEye UI-1480SE-C USB2) was mounted on a motorized linear stage in order to record the intensity profile of the beam along the propagation axis. Snapshots were taken each 2 mm: an extract of the recorded intensity profiles is shown in Fig. 5. As can be seen in the figure, the spatial quality of the beam is very good, with nearly Gaussian shape before, after, and at the focus. There is neither an existence of rings due to conical emission [10,28] nor other appreciable spatial modulations inherited from the DL focusing. From these measurements we calculated the FWHM of the beam at the different planes, as represented in Fig. 5(b). In this plot we have also represented the best-fit curve for Gaussian beam propagation. In order to account for the beam quality we estimated the quality factor, M^2, following the procedure ISO/DIS 11146. For a real beam transformed by a lens, the radius at $1/e^2$ of intensity along the propagation axis (which can be easily related to the FWHM) changes according to the following equation [29]:

$$w^2(z) = \frac{M^2\lambda}{\pi z_R}\left[z_0^2 + z_R^2 - \left(2z_0 + 2\frac{z_0^2 + z_R^2}{f}\right)z + \left(1 + \frac{2z_0}{f} + \frac{z_0^2 + z_R^2}{f^2}\right)z^2\right], \quad (3)$$

z_R being the Rayleigh length, z_0 the waist plane, f the focal length of the lens, and M^2 the quality factor. Equation (3) can thus be expressed as an algebraic expression in terms of z:

$$\omega^2(z) = a + bz + cz^2, \quad (4)$$

which allows for the calculation of M^2 as

$$M^2 = \frac{\pi}{\lambda z^2}\sqrt{ac - \frac{b^2}{4}}. \quad (5)$$

The previous equation yields an M^2 factor of 1.4.

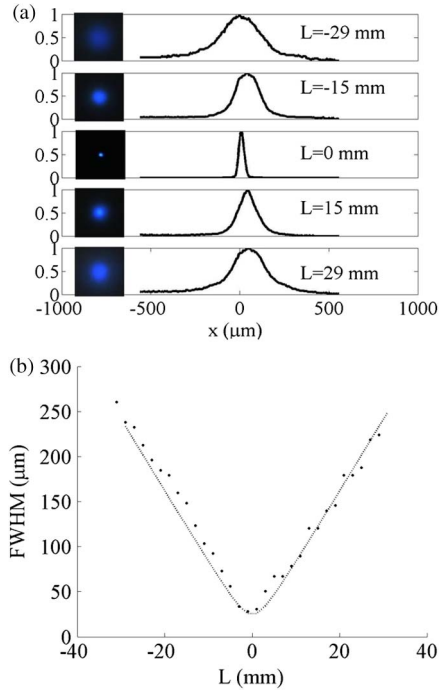

Fig. 5. (a) Spatial profiles of the SC pulse near the focus of a $f = 200$ mm lens. The sapphire crystal was placed at $z = 1.2$ mm, and the pulse energy of the IR was $E = 1.3$ μJ. (b) Measured waist of the SC pulse and fitting to a Gaussian beam.

Note that Eq. (5) depends on the wavelength. For the estimation of M^2 we have chosen $\lambda = 440$ nm (the central wavelength of the peaked blue structure). A rigorous analysis for polychromatic light can be found in [29].

When we repeated the experiment for other positions (z) of the sapphire plate such that the filament was properly developed, we observed the formation of a ring-shaped structure before the focus. To find out if the so-generated SC pulses presented chromatic aberration, we also plotted the FWHM for each channel (RGB) of the camera for the distance at which the spectral content is larger (z = 0.15 mm). The curves obtained for the three colors showed similar divergences (slightly larger for the longer wavelengths) and the same focus position, indicating that no strong chromatic aberration was induced in the generated SC pulses with a DL. For comparison purposes, a similar study was conducted for SC generation with a RL of similar focal length ($f = 100$ mm). The energy was adjusted to $1.4E_{\text{th}}$ to work in analogous conditions. We also observed a more pronounced focusing of the reddish wavelengths, associated with a larger beam divergence at those wavelengths.

C. Extension to UV and Temporal Characterization

In order to extend the tunability of the pulses to the UV, we performed a setup for SFG with the fundamental IR pulses. To this end, a sample of the 795 nm, 120 fs pulses was taken before the setup for SC generation. A length-variable motorized delay line was mounted for this beam to equalize both optical paths, and it was focused in a type-I BBO ($\theta = 44.3°$, $\phi = 90°$, 100 μm thick) through a $f = 75$ mm lens. The SC pulses were also directed toward the BBO and were focused by a concave mirror ($f = 50$ mm) in the crystal, forming an angle of ~20° with the fundamental. The pulse energy of the 795 nm pulses

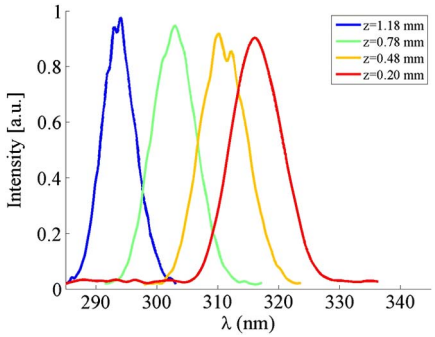

Fig. 6. Normalized spectra obtained by SFG of the SC pulses with a fundamental pulse in a BBO crystal. The position of the sapphire crystal was scanned, thus obtaining tunability of the sum-frequency pulse in the range of 290–320 nm.

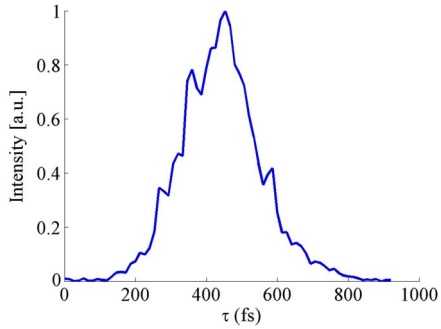

Fig. 7. Cross-correlation traces of the SC pulses generated at $z = 1.18$ mm and $E = 1.30$ μJ with the fundamental pulses. The curve has been obtained by integrating the SFG signal of the two pulses.

was attenuated with neutral-density filters in order to avoid damage of the nonlinear crystal. Once the spatial and temporal overlap was properly achieved, and the crystal was rotated to achieve the phase-matching condition ($\theta \sim 39°$), UV radiation was generated at the output of the crystals (see Fig. 6) between both beams. When we tuned the central wavelength of the SC pulses by changing the position z of the sapphire crystal, the generated UV signal was tuned accordingly. However, small adjustments of the delay line were required to optimize the temporal overlap between the two pulses and to maximize the generated signal. In Fig. 6 we can see the spectra measured for different positions of the sapphire crystal. The estimated temporal durations in the Fourier limit are 26.81 fs ($z = 1.18$ mm), 22.82 fs ($z = 0.78$ mm), 22.91 fs ($z = 0.48$ mm), and 11.41 fs ($z = 0.20$ mm).

Note that the crystal thickness yields an acceptance bandwidth slightly smaller than the SC spectral bandwidth, thus limiting the spectra of the so-generated UV pulses. In order to avoid the spectral clipping of the SC pulses, a thinner crystal should be used (~20 μm for the largest spectrum), at the expense of reducing further the efficiency of the conversion process.

This setup was used to measure the temporal duration of the SC pulses by generating the cross-correlation trace. The sapphire crystal was placed at $z = 1.18$ mm, thus obtaining the spectral peak centered at the shortest wavelength (462 nm). The relative delay between the interacting pulses was controlled with the motorized stage, which was continuously moved in steps of 2 μm while the power of the generated UV was registered. As result, the cross-correlation trace (Fig. 7) is obtained. An estimation of temporal duration of the SC pulses can be achieved by applying the expression [30]

$$\tau_{SC} = (\tau_{XC}^{p} - \tau_{IR}^{p})^{1/p}, \tag{6}$$

where τ_{XC} is the FWHM of the cross-correlation trace, τ_{IR} is the temporal duration of the fundamental pulses (120 fs), and $p = 2$ if we assume Gaussian envelopes. Then, we obtain $\tau_{SC} \sim 160$ fs, but we must take into account that there is a significant time smearing in the crystal between the IR and the blue pulses that amounts to ~20 fs; thus we expect the pulse duration of the SC pulses to be a few tens of femtoseconds shorter.

4. CONCLUSIONS

We have studied SC generation by focusing femtosecond IR pulses with a DL on a sapphire crystal. The spectral properties of the generated SC pulses can be controlled by changing the relative position of the focus in the sample, thus resulting in tunable pulses in the blue. Side-view pictures of the filament formed in the crystal have been taken with a CMOS camera, and a refocalization can be observed. The clipping of the filament in the exit face of the crystal is directly connected with the reported behavior.

The spatial properties of the generated SC pulses are analyzed for different situations. For the strongest clipping of the filament, the generated blue beam exhibits excellent spatial properties with nearly Gaussian mode. The measured M^2 parameter of the beam was 1.4, indicating a fairly good spatial quality. As the filament clipping is reduced, the spatial structure becomes worse and a ring-like structure appears. Spatial chirp and chromatic aberration were also studied, finding that both of them are negligible.

The tunability of the SC pulses is extended to the UV by SFG with the fundamental IR beam in a BBO crystal. The setup was also used to measure the temporal duration of the SC pulses by cross-correlation, and pulse lengths in the range of 150 fs are obtained. The reported study confirms the potential of using diffractive elements for triggering nonlinear optical processes in the femtosecond regime.

ACKNOWLEDGMENTS

This research was funded by the Spanish Ministerio de Ciencia e Innovación (MICINN), through Consolider Program SAUUL CSD2007-00013 and FIS2010-15746, the Junta de Castilla y León through the project SA086A12-2, the EC's Seventh Framework Programme (LASERLAB-EUROPE, grant agreement no. 228334), and the Generalitat Valenciana through project PROMETEO/2012/021. Support from the Centro de Láseres Pulsados (CLPU) is also acknowledged. R. Borrego-Varillas thanks the MICINN for funding within the FPU program (grant no. AP2007-00202).

REFERENCES

1. R. W. Boyd, *Nonlinear Optics* (Academic, 2008).
2. P. A. Franken, A. E. Hill, C. W. Peters, and G. Weinreich, "Generation of optical harmonics," Phys. Rev. Lett. **7**, 118–119 (1961).
3. F. Rotermund and V. Petrov, "Generation of the fourth harmonic of a femtosecond Ti:sapphire laser," Opt. Lett. **23**, 1040–1042 (1998).

4. G. Cerullo and S. De Silvestri, "Ultrafast optical parametric amplifiers," Rev. Sci. Instrum. **74**, 1–18 (2003).
5. K. Osvay, G. Kurdi, J. Klebniczki, M. Csatári, and I. N. Ross, "Demonstration of high gain amplification of femtosecond ultraviolet laser pulses," Appl. Phys. Lett. **80**, 1704–1706 (2002).
6. P. Tzankov, T. Fiebig, and I. Buchvarov, "Tunable femtosecond pulses in the near-ultraviolet from ultrabroadband amplification," Appl. Phys. Lett. **82**, 517–519 (2003).
7. R. R. Alfano, *The Supercontinuum Laser Source* (Springer Verlag, 2006).
8. H. Dachraoui, C. Oberer, M. Michelswirth, and U. Heinzmann, "Direct time-domain observation of laser pulse filaments in transparent media," Phys. Rev. A **82**, 043820 (2010).
9. R. R. Alfano and S. L. Shapiro, "Emission in the region 4000 to 7000 A via four-photon coupling in glass," Phys. Rev. Lett. **24**, 584–587 (1970).
10. M. Bradler, P. Baum, and E. Riedle, "Femtosecond continuum generation in bulk laser host materials with sub-μJ pump pulses," Appl. Phys. B **97**, 561–574 (2009).
11. A. Brodeur and S. L. Chin, "Band-gap dependence of the ultrafast white-light continuum," Phys. Rev. Lett. **80**, 4406–4409 (1998).
12. C. Nagura, A. Suda, H. Kawano, M. Obara, and K. Midorikawa, "Generation and characterization of ultrafast white-light continuum in condensed media," Appl. Opt. **41**, 3735–3742 (2002).
13. A. Brodeur and S. L. Chin, "Ultrafast white-light continuum generation and self-focusing in transparent condensed media," J. Opt. Soc. Am. B **16**, 637–650 (1999).
14. M. Kolesik, G. Katona, J. V. Moloney, and E. M. Wright, "Physical factors limiting the spectral extent and band gap dependence of supercontinuum generation," Phys. Rev. Lett. **91**, 043905 (2003).
15. J. B. Ashcom, R. R. Gattass, C. B. Shaffer, and E. Mazur, "Numerical aperture dependence of damage and supercontinuum generation from femtosecond laser pulses in bulk fused silica," J. Opt. Soc. Am. B **23**, 2317–2322 (2006).
16. Z. Wu, H. Jiang, Q. Sun, H. Yang, and Q. Gong, "Filamentation and temporal reshaping of a femtosecond pulse in fused silica," Phys. Rev. A **68**, 063820 (2003).
17. M. Ziolek, R. Naskrecki, and J. Karolczak, "Some temporal and spectral properties of femtosecond supercontinuum important in pump-probe spectroscopy," Opt. Commun. **241**, 221–229 (2004).
18. A. K. Dharmadhikari, F. A. Rajgara, and D. Mathur, "Systematic study of highly efficient white light generation in transparent materials using intense femtosecond laser pulses," Appl. Phys. B **80**, 61–66 (2005).
19. X. Fang and T. Kobayashi, "Evolution of a super-broadened spectrum in filament generated by an ultrashort intense laser pulse in fused silica," Appl. Phys. B **77**, 167–170 (2003).
20. C. Romero, R. Borrego-Varillas, A. Camino, G. Minguez-Vega, O. Mendoza-Yero, J. Hernández-Toro, and J. R. Vázquez de Aldana, "Diffractive optics for spectral control of the supercontinuum generated in sapphire with femtosecond pulses," Opt. Express **19**, 4977–4984 (2011).
21. V. Moreno, J. F. Román, and J. R. Salgueiro, "High efficiency diffractive lenses: deduction of kinoform profile," Am. J. Phys. **65**, 556–562 (1997).
22. G. Mínguez-Vega, C. Romero, O. Mendoza-Yero, J. R. Vázquez de Aldana, R. Borrego-Varillas, C. Méndez, P. Andrés, J. Lancis, V. Climent, and L. Roso, "Wavelength tuning of femtosecond pulses generated in nonlinear crystals by using diffractive lenses," Opt. Lett. **35**, 3694–3696 (2010).
23. H. Urey, "Spot size, depth-of-focus, and diffraction ring intensity formulas for truncated Gaussian beams," Appl. Opt. **43**, 620–625 (2004).
24. B. Alonso, R. Borrego-Varillas, O. Mendoza-Yero, I. J. Sola, J. San Román, G. Mínguez-Vega, and L. Roso, "Frequency resolved wavefront retrieval and dynamics of diffractive focused ultrashort pulses," J. Opt. Soc. Am. B **29**, 1993–2000 (2012).
25. V. Kartazaev and R. R. Alfano, "Supercontinuum generated in calcite with chirped femtosecond pulses," Opt. Lett. **32**, 3293–3295 (2007).
26. D. Faccio, A. Averchi, A. Lotti, M. Kolesik, J. V. Moloney, A. Couairon, and P. di Trapani, "Generation and control of extreme blueshifted continuum peaks in optical Kerr media," Phys. Rev. A **78**, 033825 (2008).
27. E. O. Smetanina, V. O. Kompanets, S. V. Chekalin, A. E. Dormidonov, and V. P. Kandidov, "Anti-Stokes wing of femtosecond laser filament supercontinuum in fused silica," Opt. Lett. **38**, 16–18 (2013).
28. Q. Xing, K. M. Yoo, and R. R. Alfano, "Conical emission by four-photon parametric generation by using femtosecond laser pulses," Appl. Opt. **32**, 2087–2089 (1993).
29. L. Martí-López, O. Mendoza-Yero, and J. A. Ramos de Campos, "Propagation of polychromatic Gaussian beams through thin lenses," J. Opt. Soc. Am. A **18**, 1348–1356 (2001).
30. A. P. Baronavski, H. D. Ladouceur, and J. K. Shaw, "Analysis of cross correlation, phase velocity mismatch, and group velocity mismatches in sum-frequency generation," IEEE J. Quantum Electron. **29**, 580–589 (1993).